

Comparison of spin-wave transmission in parallel and antiparallel magnetic configurations

Y. W. Xing,^{1,2,*} Z. R. Yan,^{1,*} and X. F. Han^{1,2,3,†}

¹*Beijing National Laboratory for Condensed Matter Physics,
Institute of Physics, University of Chinese Academy of Sciences,
Chinese Academy of Sciences, Beijing 100190, China*

²*Center of Materials Science and Optoelectronics Engineering,
University of Chinese Academy of Sciences, Beijing 100049, China*

³*Songshan Lake Materials Laboratory, Dongguan, Guangdong 523808, China*

(Dated: December 21, 2021)

Parallel (P) and antiparallel (AP) configurations are widely applied in magnetic heterostructures and have significant impacts on the spin-wave transmission in magnonic devices. In the present study, a theoretical investigation was conducted into the transmission of exchange-dominated spin waves with nanoscale wavelengths in a type of heterostructure including two magnetic media, of which the magnetization state can be set to the P (AP) configuration by ferromagnetic (antiferromagnetic) interfacial exchange coupling (IEC). The boundary conditions in P and AP cases were derived, by which the transmission and reflection coefficients of spin waves were analytically given and numerically calculated. In the P configuration, a critical angle θ_c always exists and has a significant influence on the transmission. Spin waves are refracted and reflected when the incident angle θ_i is smaller than the critical angle ($\theta_i < \theta_c$), while total reflection occurs as $\theta_i \geq \theta_c$. In the AP configuration, the spin-wave polarizations of medium 1 and 2 are inverse, that is, right-handed (RH) and left-handed (LH), leading to the total reflection being independent of θ_i . As demonstrated by the difference in spin-wave transmission properties between the P ($\theta_i < \theta_c$) and AP cases, there is a polarization-dependent scattering. However, as θ_i exceeds θ_c , the P ($\theta_i > \theta_c$) case exhibits similarities with the AP case, where the transmitted waves are found to be evanescent in medium 2 and their decay lengths are investigated. In both the P ($\theta_i > \theta_c$) and AP cases, the Goos-Hänchen (GH) shift of the total reflection waves are calculated and shown as a function of the frequency and incident angle. The relationship between the decay lengths and GH shifts is also explored. Further, as the number of media exceeds two, spin waves are scattered by multiple interfaces, resulting in the resonant transmission effect in the P ($\theta_i < \theta_c$) case. At the same time, there is a tunnelling effect and a resonant tunnelling effect in the P ($\theta_i > \theta_c$) and AP cases, which are attributed to the evanescent waves. The influences of the IEC strength on all of the aforementioned findings are investigated in detail. The present study provides a comprehensive guide for the transmission of spin waves in the magnetic systems with either P or AP configuration and is helpful for the design of future magnonic devices.

I. INTRODUCTION

In the field of traditional spintronics, the relative orientation of magnetizations has a significant impact on the transport properties of electrons, such as the different magnetoresistance between parallel (P) and antiparallel (AP) configurations in the spin valves^{1,2} and magnetic tunneling junctions (MTJs)³⁻⁵. In 1975, Jullire studied the conductance of Fe/Ge/Co junctions at 4.2 K in P and AP states³. The difference in conductance between the two states demonstrated that the scattering of electrons is spin-dependent, which is referred to as tunneling magnetoresistance (TMR).

The application of such magnetoresistance effect in technology is difficult due to the necessity of low temperature. In the late 1980s, giant magnetoresistance (GMR) was discovered by Fert¹ and Grünberg², which greatly facilitated further researches and applications, and is generally regarded as the beginning of spintronics⁶. The ferromagnetic/nonmagnetic/ferromagnetic sandwiches are the key structures for realizing GMR, of which the resistance exhibits a significant change between the P and

AP states at both low and room temperatures. Subsequently, a type of spin valve was proposed in respect of the antiferromagnetic pinning⁷⁻¹⁰, which is extensively used in magnetic read heads and sensors. In 1995, the room-temperature TMR was discovered by Miyazaki⁴ and Moodera⁵ in MTJs with the Al₂O₃ insulating barrier. Such discovery further promoted the development of spintronics.

Inspired by the effects of GMR and TMR, studies have been conducted regarding the transmission properties of other particles or quasi-particles in P and AP configurations, such as magnons. As the elementary excitation of the magnetic system, spin waves, or magnons, are regarded as potential information carriers. The research field of magnons is called magnonics¹¹⁻¹⁵, in which the kernel is to manipulate the magnon transmission by various designs¹⁶⁻²⁷. Among these researches, Wu *et al.*²⁰ fabricated a new type of device, YIG/Au/YIG, which was called the magnon valve and drew widespread attention. Referred to as the magnon valve effect (MVE), magnon currents can pass through the magnon valve in the P state, but are blocked in the AP state. After, the magnon

junction, YIG/NiO/YIG, was proposed²¹ as the counterpart of MTJs due to the insulating barrier. The aforementioned studies demonstrated the significant influence of magnetic configurations on the spin-wave transmission.

Notably, spin waves are thermally excited by the spin Seebeck effect (SSE) in magnon valve²⁰ and magnon junction²¹ experiments, thus the coherence of spin waves is ignored. In fact, the coherence is significant for spin-wave transmission because certain phenomena can occur, such as refraction^{28–34}, skin effect³⁵, total reflection and decay³⁶, Goos-Hänchen (GH) shift^{37–40}, tunneling⁴¹, resonant tunneling^{42,43} and resonant transmission^{44–47}. Among these works, the present authors³⁵ and Poimanov *et al.*³⁶ have investigated the transmission properties of spin waves in the AP configuration and found the evanescent waves induced by the inverse polarization, which were significantly different with the P ($\theta_i < \theta_c$) case. However, few studies were reported on evanescent waves in the P configuration with $\theta_i > \theta_c$. Hence, the systematic research on the transmission of coherent spin waves in P and AP magnetic configurations is essential.

In the present study, the focus is on the coherent exchange-dominated spin waves (wavelength $\lambda < 100$ nm)^{48,49}, which are significant for the nanoscale magnonic devices. The main system of the present research is comprised of two magnetic media and has two states, including the P and AP configurations, corresponding to the ferromagnetic and antiferromagnetic interfacial exchange coupling (IEC), respectively. The boundary conditions at the interface between two media were analytically deduced in both the P and AP cases. Based on the boundary conditions, the expressions of transmission and reflection coefficients were obtained. The computed results show obvious differences between the P and AP states. In the P state, the critical angle θ_c is found to always exist. When the incident angle θ_i is smaller than the critical angle θ_c , spin waves are refracted and reflected. When $\theta_i \geq \theta_c$, spin waves are all reflected. In the AP state, there is no critical angle and total reflection invariably occurs. Such findings can be attributed to the inverse spin-wave polarizations of medium 1 and 2, that is, right-handed (RH) and left-handed (LH). Further, in the cases of total reflection in both the P and AP states, the spin waves are found to penetrate into medium 2 in the form of evanescent waves. The decay lengths of such evanescent waves are analytically and numerically studied. The relationship between the decay lengths and GH shifts is also explored. Additionally, the spin waves propagating in multiple media are investigated, in which the phenomena of resonant transmission, tunnelling and resonant tunnelling occur.

II. ANALYTICAL MODEL

As shown in Figure 1(a), a system of two magnetic media is considered with \mathbf{m}_n ($n = 1$ or 2) being the unit

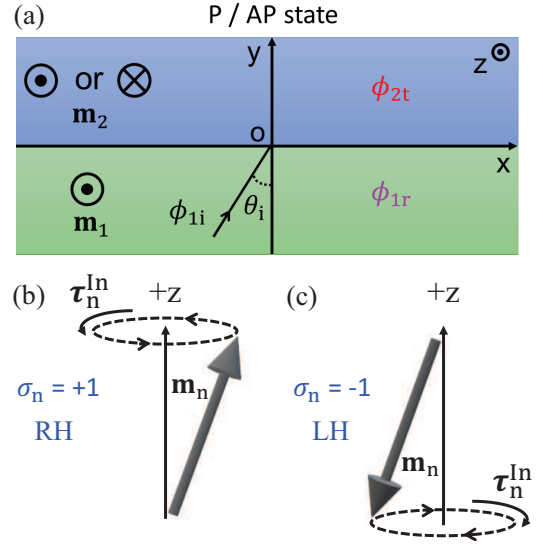


FIG. 1. (a) The schematic diagram of the two-medium system in the P or AP state. \mathbf{m}_1 is in the $+z$ direction, while \mathbf{m}_2 is along $+z$ ($-z$) in the P (AP) state. ϕ_{1i} and ϕ_{1r} represent the incident and reflected waves in medium 1, while ϕ_{2t} denotes the transmitted waves in medium 2. θ_i is the incident angle and the incident point is the origin of coordinates. (b) and (c) show the RH and LH spin-wave polarizations, corresponding to $\sigma_n = +1$ and -1 , respectively.

magnetization vector. The magnetic media can be either ferromagnetic or ferrimagnetic in the model. The type of IEC between medium 1 and 2 can be ferromagnetic and antiferromagnetic⁵⁰, corresponding to P ($A_{12} > 0$) and AP ($A_{12} < 0$) states with A_{12} being the constant of IEC. The dynamics of \mathbf{m}_n is governed by the Landau-Lifshitz-Gilbert (LLG) equation^{51,52}

$$\frac{\partial \mathbf{m}_n}{\partial t} = -\gamma \mu_0 \mathbf{m}_n \times \mathbf{H}_n^{\text{eff}} + \alpha \mathbf{m}_n \times \frac{\partial \mathbf{m}_n}{\partial t}, \quad (1)$$

where $\gamma = 1.76 \times 10^{11}$ rad/(s T) is the gyromagnetic ratio, μ_0 is the vacuum permeability, α is the Gilbert damping coefficient, $\mu_0 \mathbf{H}_n^{\text{eff}} = \frac{2A_n}{M_n} \nabla^2 \mathbf{m}_n + \sigma_n \frac{2K_n}{M_n} \mathbf{e}_z$ is the effective field with the saturation magnetization M_n , exchange constant A_n and uniaxial magnetic anisotropy constant K_n , and σ_n is the orientation factor of \mathbf{m}_n . As shown in Figure 1(b) and (c), if $\sigma_n = +1$ (-1), \mathbf{m}_n is parallel (antiparallel) to $+z$ axis, representing that the spin-wave polarization of the medium is RH (LH). The internal torque is $\tau_n^{\text{In}} = -\gamma \mu_0 \mathbf{m}_n \times \mathbf{H}_n^{\text{eff}}$. For an independent spin-up or spin-down medium, the internal spin waves are right-handed circularly polarized (RHCP) or left-handed circularly polarized (LHCP). However, due to the IEC, the situation gets complicated for a system of two coupled media.

In the P (AP) state of the two-medium system, $\sigma_1 = \sigma_2 = +1$ ($\sigma_1 = +1$ and $\sigma_2 = -1$), and the spin-wave polarizations of medium 1 and 2 are the same (inverse). In order to solve the problem of spin-wave propagation in the system, the boundary conditions at the interface

($y = 0$) need to be derived. A disk is considered that covers the part from $y = -\varepsilon$ to $y = 0$ with the thickness $\varepsilon \ll 1$ and the cross section area being ξ . Integrating Eq. (1) over the volume of the disk and neglecting the damping α , one can get^{45,53}

$$I_{\text{ex}} + I_{\text{IEC}} = 0, \quad (2)$$

where

$$\begin{aligned} I_{\text{ex}} &= \int \mathbf{m}_1 \times \mathbf{H}_{\text{ex},1} dV \\ &= \frac{2A_1}{\mu_0 M_1} \int \mathbf{m}_1 \times \nabla^2 \mathbf{m}_1 dV \\ &= -\xi \frac{2A_1}{\mu_0 M_1} \mathbf{m}_1 \times \frac{\partial \mathbf{m}_1}{\partial y} \end{aligned} \quad (3)$$

and

$$\begin{aligned} I_{\text{IEC}} &= \int \mathbf{m}_1 \times \mathbf{H}_{\text{IEC},1} dV \\ &= \frac{2A_{12}}{\mu_0 M_1 \varepsilon} \int \mathbf{m}_1 \times \mathbf{m}_2 dV \\ &= \xi \frac{2A_{12}}{\mu_0 M_1} \mathbf{m}_1 \times \mathbf{m}_2 \end{aligned} \quad (4)$$

are the only terms which can not be neglected. Uniting Eq. (2)-(4), it leads to

$$A_1 \mathbf{m}_1 \times \frac{\partial \mathbf{m}_1}{\partial y} = A_{12} \mathbf{m}_1 \times \mathbf{m}_2. \quad (5)$$

Similarly, another disk can be considered that covers the part from $y = 0$ to $y = \varepsilon$ with the thickness $\varepsilon \ll 1$ and the cross section area being ξ . Integrating Eq. (1) over the volume of this disk and neglecting the damping, the following equations can be obtained⁴⁵:

$$I'_{\text{ex}} + I'_{\text{IEC}} = 0, \quad (6)$$

where

$$\begin{aligned} I'_{\text{ex}} &= \int \mathbf{m}_2 \times \mathbf{H}_{\text{ex},2} dV \\ &= \frac{2A_2}{\mu_0 M_2} \int \mathbf{m}_2 \times \nabla^2 \mathbf{m}_2 dV \\ &= \xi \frac{2A_2}{\mu_0 M_2} \mathbf{m}_2 \times \frac{\partial \mathbf{m}_2}{\partial y} \end{aligned} \quad (7)$$

and

$$\begin{aligned} I'_{\text{IEC}} &= \int \mathbf{m}_2 \times \mathbf{H}_{\text{IEC},2} dV \\ &= \frac{2A_{12}}{\mu_0 M_2 \varepsilon} \int \mathbf{m}_2 \times \mathbf{m}_1 dV \\ &= \xi \frac{2A_{12}}{\mu_0 M_2} \mathbf{m}_2 \times \mathbf{m}_1. \end{aligned} \quad (8)$$

Uniting Eq. (6)-(8), it leads to

$$A_2 \mathbf{m}_2 \times \frac{\partial \mathbf{m}_2}{\partial y} = A_{12} \mathbf{m}_1 \times \mathbf{m}_2. \quad (9)$$

Eq. (5) and Eq. (9) are the complete boundary conditions, and thus can be rewritten together as^{29,34,45}

$$\begin{cases} A_1 \mathbf{m}_1 \times \frac{\partial \mathbf{m}_1}{\partial y} = A_{12} \mathbf{m}_1 \times \mathbf{m}_2 \\ A_2 \mathbf{m}_2 \times \frac{\partial \mathbf{m}_2}{\partial y} = A_{12} \mathbf{m}_1 \times \mathbf{m}_2. \end{cases} \quad (10)$$

A small fluctuation of \mathbf{m}_n with $\mathbf{m}_n = \mathbf{m}_{0,n} + \tilde{\mathbf{m}}_n$ is assumed, where $\mathbf{m}_{0,1} = +\mathbf{e}_z$, $\mathbf{m}_{0,2} = +\mathbf{e}_z$ in the P state and $\mathbf{m}_{0,1} = +\mathbf{e}_z$, $\mathbf{m}_{0,2} = -\mathbf{e}_z$ in the AP state, $\tilde{\mathbf{m}}_n = (m_{x,n}, m_{y,n}, 0)$ and $|\mathbf{m}_n| \ll 1$. In the P case, replacing \mathbf{m}_n with $\mathbf{m}_{0,n} + \tilde{\mathbf{m}}_n$ in Eq. (10) and keeping the linear terms of $\tilde{\mathbf{m}}_n$ leads to the boundary conditions⁴⁵

$$\begin{cases} A_1 \frac{\partial \tilde{\mathbf{m}}_1}{\partial y} + A_{12}(\tilde{\mathbf{m}}_1 - \tilde{\mathbf{m}}_2) = 0 \\ A_2 \frac{\partial \tilde{\mathbf{m}}_2}{\partial y} + A_{12}(\tilde{\mathbf{m}}_1 - \tilde{\mathbf{m}}_2) = 0. \end{cases} \quad (11)$$

In the AP case, the boundary conditions can be written as

$$\begin{cases} A_1 \frac{\partial \tilde{\mathbf{m}}_1}{\partial y} - A_{12}(\tilde{\mathbf{m}}_1 + \tilde{\mathbf{m}}_2) = 0 \\ -A_2 \frac{\partial \tilde{\mathbf{m}}_2}{\partial y} - A_{12}(\tilde{\mathbf{m}}_1 + \tilde{\mathbf{m}}_2) = 0. \end{cases} \quad (12)$$

Considering a negligible damping α and defining a spin-wave function $\psi_n(x, t) = m_{x,n}(x, t) - im_{y,n}(x, t)$, the LLG Eq. (1) can be recasted into an effective Schrödinger equation^{31,40,54-59}

$$i\hbar \frac{\partial \psi_n}{\partial t} = H_n \psi_n = \left(\frac{\hat{p}^2}{2m_n^*} + V_n \right) \psi_n, \quad (13)$$

where $\hat{p} = -i\hbar \nabla$ is the momentum operator and $m_n^* = \hbar M_n / 4\gamma m_{z,n} A_n = \hbar M_n / 4\gamma \sigma_n A_n$ is the effective mass of magnons. $V_n = 2\gamma \hbar \sigma_n K_n / M_n$ represents the potential energy. From Eq. (13), the spin-wave dispersion relation can be obtained³⁵:

$$\begin{aligned} \omega_n &= E_n / \hbar \\ &= (\frac{p_n^2}{2m_n^*} + V_n) / \hbar \\ &= \frac{\hbar}{2m_n^*} k_n^2 + 2\gamma \sigma_n K_n / M_n, \end{aligned} \quad (14)$$

where $k_n^2 = \mathbf{k}_n \cdot \mathbf{k}_n$, which shows the magnitude of wave vectors. The sign of ω_n is obviously positive (negative) as $\sigma_n = +1(-1)$, indicating that the spin-wave polarization is RH (LH).

For simplicity, a normalized wave function is defined as $\hat{\psi}_n(x, t) = \psi_n(x, t) / |\psi_{1i}(x, t)|$, where $|\psi_{1i}(x, t)|$ represents the amplitude of the incident waves in medium 1, ensuring that $|\hat{\psi}_n(x, t)| = 1$. Then the space and time part of $\hat{\psi}_n(x, t)$ are separated via $\hat{\psi}_n(x, t) = \phi_n(x) e^{-i\omega t}$.

From Eq. (11) and Eq. (12), the boundary conditions of $\phi_n(x)$ can be obtained and written as

$$\begin{cases} A_1 \frac{\partial \phi_1}{\partial y} + A_{12}(\phi_1 - \phi_2) = 0 \\ A_2 \frac{\partial \phi_2}{\partial y} + A_{12}(\phi_1 - \phi_2) = 0 \end{cases} \quad (15)$$

and

$$\begin{cases} A_1 \frac{\partial \phi_1}{\partial y} - A_{12}(\phi_1 + \phi_2) = 0 \\ -A_2 \frac{\partial \phi_2}{\partial y} - A_{12}(\phi_1 + \phi_2) = 0, \end{cases} \quad (16)$$

corresponding to the P and AP cases, respectively.

The following assumptions can be made that $\phi_1(x) = \phi_{1i}(x) + \phi_{1r}(x) = e^{i(k_x^i x + k_y^i y)} + r e^{i(k_x^r x + k_y^r y)}$ and $\phi_2(x) = \phi_{2t}(x) = t e^{i(k_x^t x + k_y^t y)}$ with r and t being the reflection and transmission coefficients. $\mathbf{k}^i = (k_x^i, k_y^i)$, $\mathbf{k}^r = (k_x^r, k_y^r)$ and $\mathbf{k}^t = (k_x^t, k_y^t)$ are the wave vectors of incident, reflected and transmitted waves, respectively. Thus, the relations $(\mathbf{k}^i)^2 = (\mathbf{k}^r)^2 = (k_1)^2$ and $(\mathbf{k}^t)^2 = (k_2)^2$ can be obtained. The tangential component of the wave vector is conserved due to the translational symmetry along the interface^{40,60,61}, $k_x^i = k_x^r = k_x^t$. According to the aforementioned analysis, a significant relation is obtained, $k_y^i = -k_y^r$. Hence, the reflected angle θ_r must be equal to the incident angle θ_i , which is called the law of reflection. In the P state, via Eq. (15), the reflection and transmission coefficients can be derived as

$$r_P = \frac{A_1 A_2 k_y^i k_y^t + i A_1 A_{12} k_y^i - i A_2 A_{12} k_y^t}{A_1 A_2 k_y^i k_y^t + i A_1 A_{12} k_y^i + i A_2 A_{12} k_y^t} \quad (17)$$

and

$$t_P = \frac{2i A_1 A_{12} k_y^i}{A_1 A_2 k_y^i k_y^t + i A_1 A_{12} k_y^i + i A_2 A_{12} k_y^t}. \quad (18)$$

In the uniform medium, generally, $r_P^2 + t_P^2 = 1$ ⁴⁶. However, in the present system of two different media, $r_P^2 + t_P^2 \neq 1$, due to the amplitude of reflected waves r_P being normalized to that of incident waves in medium 1, but not t_P . Thus, the reflectance and transmittance are defined as $R = r_P^2$ and $T = 1 - r_P^2 = 1 - R$, respectively. Notably, t_P represents the amplitude of transmitted waves. A detailed discussion of R and T is provided in Section III, A. $R, T \in (0,1)$ and the refraction of spin waves occurs when the incident angle is less than critical angle ($\theta_i < \theta_c$). As θ_i reaches or exceeds θ_c ($\theta_i \geq \theta_c$), $R \equiv 1$ and $T \equiv 0$, the total reflection occurs in medium 1 and the transmitted waves become evanescent in medium 2.

In the AP state, via Eq. (16), the following equations can be obtained:

$$r_{AP} = \frac{A_1 A_2 k_y^i k_y^t - i A_1 A_{12} k_y^i + i A_2 A_{12} k_y^t}{A_1 A_2 k_y^i k_y^t - i A_1 A_{12} k_y^i - i A_2 A_{12} k_y^t} \quad (19)$$

and

$$t_{AP} = \frac{2i A_1 A_{12} k_y^i}{A_1 A_2 k_y^i k_y^t - i A_1 A_{12} k_y^i - i A_2 A_{12} k_y^t}. \quad (20)$$

Here, k_y^t is a pure imaginary number, according to Eq. (14). $R = r_{AP}^2 \equiv 1$ and $T = 1 - R \equiv 0$, indicating that total reflection invariably occurs, similar to the magnon blocking effect in magnon junctions⁶². Here, $\phi_{2t}(x) = t_{AP} e^{-|k_y^t| y} e^{i k_x^t x} = t_{AP} e^{-\frac{y}{L_{12}}} e^{i k_x^t x}$ is an evanescent wave along y axis with

$$L_{12} = 1/|k_y^t| \quad (21)$$

being the decay length as spin waves propagate from medium 1 to 2. A detailed discussion of spin-wave transmission in AP state is provided in Section III, B.

In order to provide a brief understanding of the main difference between the P and AP states, the precession of magnetization near the interface is shown in Figure 2(a) and Figure 2(b). In the P state, \mathbf{m}_1 applies a torque $\boldsymbol{\tau}_{12}^{IEC} = -\gamma \mu_0 \mathbf{m}_2 \times \mathbf{H}_{IEC,2}$ on \mathbf{m}_2 due to the IEC. The spin-wave polarization caused by $\boldsymbol{\tau}_{12}^{IEC}$ is RH and the same as that caused by $\boldsymbol{\tau}_2^{In}$, leading to a plane wave $\phi_{2t}(x) = t_P e^{i(k_x^t x + k_y^t y)}$ in medium 2. By comparison, in the AP state, the spin-wave polarization caused by $\boldsymbol{\tau}_{12}^{IEC}$ is still RH but that caused by $\boldsymbol{\tau}_2^{In}$ is LH^{35,36}. For the magnetization far away from the interface, $\boldsymbol{\tau}_{12}^{IEC}$ disappears and $\boldsymbol{\tau}_2^{In}$ will be the resistance of precession, resulting in an evanescent wave $\phi_{2t}(x) = t_{AP} e^{-\frac{y}{L_{12}}} e^{i k_x^t x}$ along the y

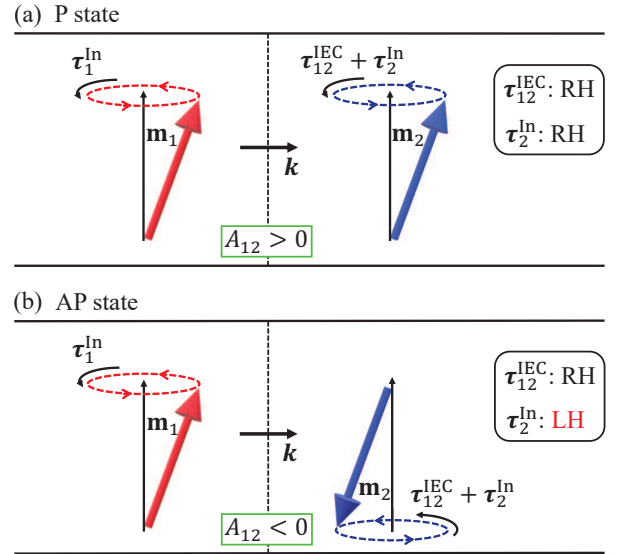


FIG. 2. The spin dynamics at the interface in the P and AP states. (a) The precession details of \mathbf{m}_1 (red) and \mathbf{m}_2 (blue) at the interface between two magnetic media with the P configuration, where the type of IEC is ferromagnetic ($A_{12} > 0$). (b) shows the case of the AP configuration, where the IEC is antiferromagnetic ($A_{12} < 0$). The vector \mathbf{k} represents the spin-wave propagation direction.

direction. Therefore, the spin-wave transmission properties are considerably different in the P and AP states.

III. RESULTS AND DISCUSSION

As discussed in this section, YIG and GdIG are chosen as medium 1 and 2, respectively. The magnetic parameters used in the calculation are as follows: the saturation magnetization, exchange constants and uniaxial magnetic anisotropy constants are $M_1 = 1.5 \times 10^5$ A/m, $A_1 = 3.6 \times 10^{-12}$ J/m, $K_1 = 10$ J/m³ for YIG^{63–65}, and $M_2 = 0.3 \times 10^5$ A/m, $A_2 = 3 \times 10^{-12}$ J/m, $K_2 = 4000$ J/m³ for GdIG^{66–68}. The constant of IEC between YIG and GdIG is $A_{12} = 3.3 \times 10^{-3}$ J/m² for the P configuration and $A_{12} = -3.3 \times 10^{-3}$ J/m² for the AP configuration^{37,69}.

A. P configuration

A two-medium system is first considered in the P configuration, including YIG (\mathbf{m}_1) and GdIG (\mathbf{m}_2), as shown in Figure 3(a). The frequency $\omega/2\pi$ ranges from 30 to 1000 GHz to ensure that spin waves are exchange-dominated in the system, which has been strictly demonstrated in previous research by the present authors³⁵. Reflection and refraction occur when the incident angle is less than the critical angle ($\theta_i < \theta_c$). The reflected angle θ_r is invariably equal to the incident angle θ_i , due to the law of reflection as aforementioned. The refracted angle θ_t can be obtained by the relation

$$k_1 \sin(\theta_i) = k_2 \sin(\theta_t), \quad (22)$$

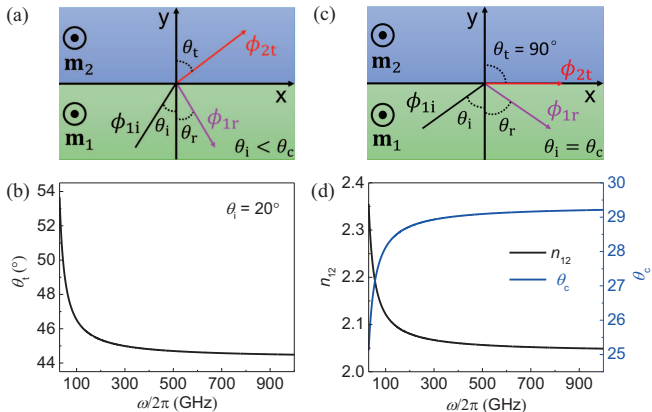


FIG. 3. The spin-wave transmission and reflection at the interface between YIG (\mathbf{m}_1) and GdIG (\mathbf{m}_2) with the P configuration. (a) When the incident angle is less than critical angle ($\theta_i < \theta_c$), spin waves are refracted and reflected. The frequency-dependent refracted angle θ_t is shown in (b) at $\theta_i = 20^\circ$. (c) As θ_i is increased to θ_c , spin waves are all reflected. (d) shows the frequency dependence of magnetic refractive index n_{12} (black) and critical angle θ_c (blue).

which is the law of refraction for spin waves, or referred to as the magnonic Snell's law^{28–34}. Figure 3(b) is the θ_t - $\omega/2\pi$ curve at $\theta_i = 20^\circ$. With the increase of $\omega/2\pi$, θ_t decreases, indicating that the spin-wave path is deflected more in the lower frequency range. As θ_t is increased to 90° , there are no refracted waves and spin waves are all reflected back, as shown in Figure 3(c). Thus, the critical angle θ_c can be obtained by $k_1 \sin(\theta_c) = k_2 \sin(90^\circ)$, leading to

$$\theta_c = \arcsin\left(\frac{k_2}{k_1}\right). \quad (23)$$

To characterize the extent of refraction, a magnetic refractive index can be defined as

$$n_{12} = 1/\sin(\theta_c) = \frac{k_1}{k_2}. \quad (24)$$

Figure 3(d) shows the magnetic refractive index n_{12} (black) and critical angle θ_c (blue) as a function of $\omega/2\pi$, demonstrating that as the frequency becomes higher, the critical angle becomes larger and the magnetic refractive index becomes smaller.

The T - $\omega/2\pi$ curves are calculated at different θ_i , as shown in Figure 4. When the incident waves are normal to the interface ($\theta_i = 0^\circ$), the transmittance T as a function of frequency $\omega/2\pi$ is shown in Figure 4(a). Notably, the transmission spectra depend on the value of A_{12} , which is discussed in the Supplemental Material⁷⁰. In Figure 4(a)-(c), as θ_i is increased, the transmittance T decreases, indicating that spin waves are more likely to pass through the interface with the smaller incident angle. As θ_i is further increased to 28° and 29° in Figure 4(d) and (e), the transmission spectra are divided into two intervals. The total reflection occurs in the low-frequency interval due to the increased n_{12} in such a range, while the high-frequency spin waves can propagate into GdIG. In Figure 4(f), as θ_i is increased to 30° , the transmittance T is zero, which means that all the spin waves in 30-1000 GHz range are totally reflected.

In the case of $\theta_i > \theta_c$, the transmitted spin waves are no longer plane waves, but evanescent waves. The anal-

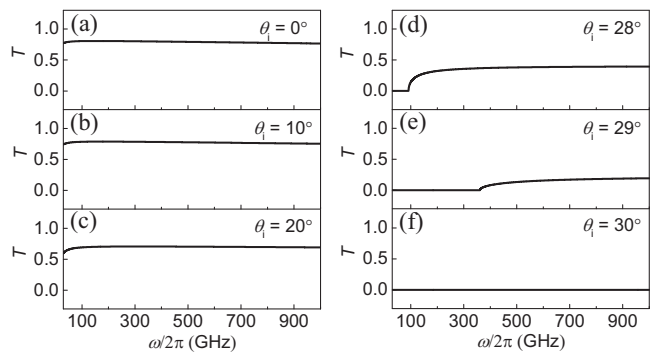


FIG. 4. The transmission spectra of spin waves in YIG (\mathbf{m}_1)/GdIG (\mathbf{m}_2) heterojunction with the P configuration. (a)-(f) show the cases of $\theta_i = 0^\circ, 10^\circ, 20^\circ, 28^\circ, 29^\circ,$ and 30° .

ogous phenomenon has been extensively investigated in optics^{71–74}, wherein the light waves turn into evanescent waves when $\theta_i > \theta_c$. In the present two-medium system, according to $(\mathbf{k}^i)^2 = (k_1)^2$, $(\mathbf{k}^t)^2 = (k_2)^2$, $k_x^i = k_x^t$ as well as $\theta_i > \theta_c$, a conclusion can be drawn that k_y^t is a pure imaginary number. As a result, $\phi_{2t}(x) = \phi_{2t}^e(x) = t_P e^{-|k_y^t|y} e^{ik_x^t x} = t_P e^{-\frac{y}{L_{12}}} e^{ik_x^t x}$, which is an evanescent wave along y axis with $L_{12} = 1/|k_y^t|$ representing the decay length of spin waves propagating from YIG (\mathbf{m}_1) to GdIG (\mathbf{m}_2). In Figure 5(a), the red dashed line represents the evanescent waves. YIG (\mathbf{m}_1) and GdIG (\mathbf{m}_2) are semi-infinite, and thus the evanescent waves will decay to infinity after departing from the interface. The calculation result of the decay length L_{12} is shown in Figure 5(b). L_{12} obviously depends on the incident angle θ_i and spin-wave frequency $\omega/2\pi$. The minimum of θ_i is 30° , ensuring $\theta_i > \theta_c$ in 30-1000 GHz. As θ_i is increased from 30° to the vicinity of 90° , L_{12} decreases monotonically. L_{12} characterizes the decay length along y instead of x axis. As a consequence, spin waves will decay more quickly in the y direction if \mathbf{k}^t is inclined to the x axis as θ_i is increased. The frequency dependence of L_{12} is also monotonic. The data reveal that spin waves tend to have longer decay lengths in the low-frequency range. As $\omega/2\pi$ is increased, the evanescent waves are more concentrated at the interface. This monotonicity is similar to the skin effect of electromagnetic waves in the air-metal system, which can be referred to as the magnonic skin effect (MSE)³⁵. Notably, the MSE was first reported in YIG/GdIG heterojunction with the AP configuration, where the MSE is applicable for $\theta_i \in [0^\circ, 90^\circ)$ without the limit of the critical angle θ_c . By contrast, the MSE occurs at $\theta_i \in [\theta_c, 90^\circ)$ in the P case.

Here, an observation can be made that the characteristics of spin-wave transmission in the P and AP configurations are not always different. The distinction and connection depend on the scope of θ_i . For the AP state, spin waves are all reflected and only the evanescent waves

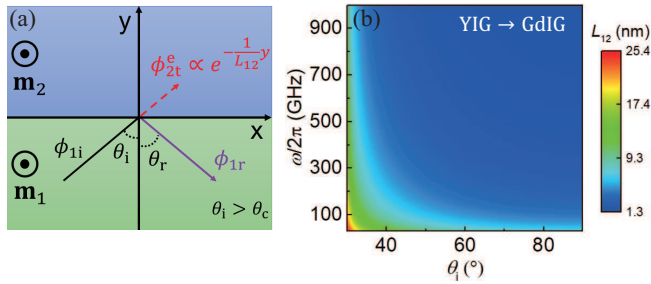


FIG. 5. The decay lengths of evanescent waves in the case of $\theta_i > \theta_c$. (a) As the incident angle θ_i exceeds the critical angle θ_c , spin waves are all reflected back. The transmitted waves are evanescent, which have the form of $e^{-\frac{y}{L_{12}}}$ in the y direction with L_{12} being the decay length as spin waves propagate from YIG (\mathbf{m}_1) to GdIG (\mathbf{m}_2). (b) shows the calculation result of the decay length L_{12} , which is dependent of the incident angle and frequency.

penetrate through the interface as $\theta_i \in [0^\circ, 90^\circ)$. For the P state, when $\theta_i \in [0^\circ, \theta_c)$, spin waves can propagate into GdIG (\mathbf{m}_2) in the form of plane waves and are partly reflected back to YIG (\mathbf{m}_1). When $\theta_i \in (\theta_c, 90^\circ)$, total reflection occurs and the spin waves penetrate through the interface in the form of decay, which are the same as those in the AP state. Attention should be paid to the value of k_y^t , which is central to understanding the aforementioned phenomena. In the AP state, k_y^t is a pure imaginary number, causing the total reflection to be $R = r_P^2 \equiv 1$ according to Eq. (19). For the small θ_i cases in the P state, k_y^t is a real number, showing the different manifestation compared with the AP state. As θ_i overtakes θ_c , k_y^t turns into a pure imaginary number, resulting in resemblance to the AP case.

In general, the GH effect occurs when spin waves are scattered at the interface^{37–40}, describing the shift between the reflected (or transmitted) point and the incident point. According to previous studies, the sign of GH shifts can be positive or negative, depending on the reflection (or transmission) coefficients. As $\theta_i > \theta_c$, the GH shift of the totally reflected spin waves can be calculated by^{37–40}

$$\Delta_r^{12} = -\frac{\partial \varphi_r}{\partial k_x^i}, \quad (25)$$

where $\varphi_r = \arctan[\text{Im}(r_P)/\text{Re}(r_P)]$ is the phase difference between the reflected and incident waves. $\text{Re}(r_P)$ and $\text{Im}(r_P)$ are the real and imaginary parts of the reflection coefficient r_P , respectively. Figure 6(a) shows the

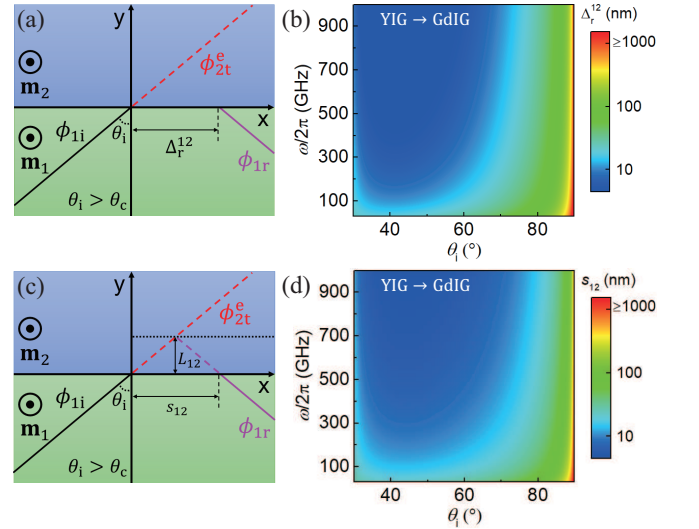


FIG. 6. The GH effect at the interface in the case of $\theta_i > \theta_c$. (a) shows the GH shift of the reflected waves, marked with Δ_r^{12} . (b) is the result of Δ_r^{12} calculated by Eq. (25), which depends on θ_i and $\omega/2\pi$. (c) shows the relationship between the lateral shift s_{12} and decay length L_{12} . The black dot line represents the effective reflecting interface. (d) The result of s_{12} calculated by Eq. (26). The color bars in (b) and (d) are shown in the log scale.

schematic of the GH shift Δ_r^{12} when spin waves propagate from YIG (\mathbf{m}_1) to GdIG (\mathbf{m}_2). Figure 6(b) shows the computed result of Δ_r^{12} as a function of θ_i and $\omega/2\pi$. An observation can be made that all the values of Δ_r^{12} are positive, ranging from several nanometers to micron scales. The frequency dependence of Δ_r^{12} is monotonic, indicating that high-frequency waves tend to have smaller GH shifts. Although the relation between Δ_r^{12} and θ_i is non-monotonic, Δ_r^{12} increases as θ_i is increased in most of the region. In particular, Δ_r^{12} goes to infinity as θ_i is close to 90° , showing a divergence and being consistent with the results of previous studies^{37,40}. Hence, for the design of spin-wave devices, the GH shift must be considered if θ_i is large.

The underlying physics of the positive GH shift should be considered beyond the mathematical calculation of Eq. (25). The positive GH shift is assumed to originate from the displacement of the effective reflecting interface, as shown in Figure 6(c). The reflection does not occur as soon as the incident waves reach the x axis. A possible scenario is that spin waves penetrate into GdIG in the form of decay and are reflected at another effective interface, resulting in a positive shift s_{12} of the reflected point along x axis. The effective reflecting interface is represented by the black dot line and the displacement is assumed as the decay length L_{12} . The following equation is evident:

$$s_{12} = 2L_{12} \tan(\theta_i). \quad (26)$$

In order to verify reasonability of the assumption, the computed result of s_{12} is shown in Figure 6(d), serving as a contrast to Δ_r^{12} in Figure 6(b). The color bars are shown in the log scale due to the divergence in the vicinity of $\theta_i = 90^\circ$. An observation can be made that there is a slight difference in the magnitude of s_{12} and Δ_r^{12} . Despite such difference, the incident-angle and frequency dependence are consistent. The comparability demonstrates that the present assumption is reasonable to some extent. Thus, conclusion can be drawn that the positive GH shift can be attributed to the penetration of the evanescent waves in GdIG, and the decay length is roughly equal to the displacement of the effective reflecting interface. Notably, Δ_r^{12} is a function of A_{12} , but s_{12} is independent of A_{12} . s_{12} and Δ_r^{12} are approximately equal, since A_{12} is relatively large. If A_{12} tends to zero, Δ_r^{12} is also decreased to zero. The influence of A_{12} on the GH shift Δ_r^{12} is shown in the Supplemental Material⁷⁰. Such findings demonstrate that Δ_r^{12} can be explained by s_{12} when the IEC between YIG and GdIG is strong.

Beyond investigating the scattering problems at a single interface in the two-medium systems, in the following, the spin-wave scattering at multiple interfaces in the multi-medium systems is explored. The YIG (\mathbf{m}_1)/GdIG (\mathbf{m}_2)/YIG (\mathbf{m}_3) heterostructure is first considered, as shown in Figure 7(a) with $\theta_i < \theta_c$ and Figure 7(e) with $\theta_i > \theta_c$. In the case of $\theta_i < \theta_c$, the incident waves are refracted and reflected at two interfaces. Via the transfer matrix method (TMM)^{46,75,76}, the transmission co-

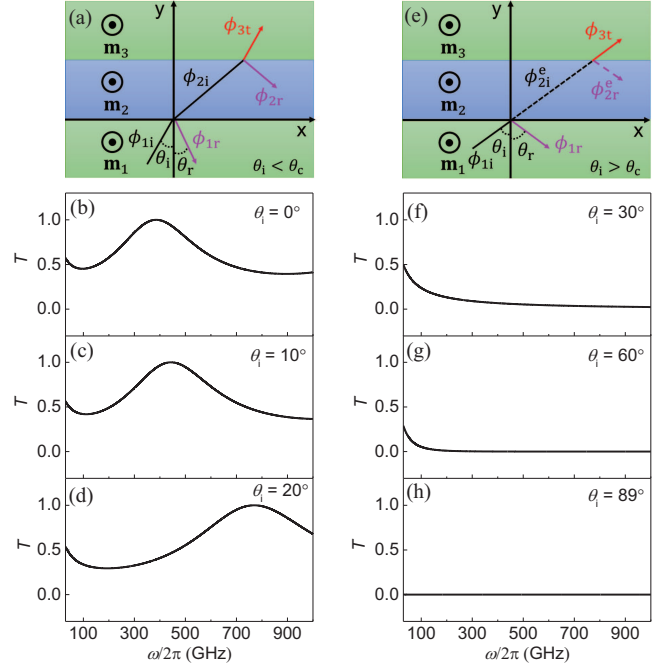


FIG. 7. The transmission spectra of spin waves in YIG (\mathbf{m}_1)/GdIG (\mathbf{m}_2)/YIG (\mathbf{m}_3) with the P configuration. (a)-(d) and (e)-(h) correspond to the cases of $\theta_i < \theta_c$ and $\theta_i > \theta_c$, respectively. (a) In the case of $\theta_i < \theta_c$, the spin waves are refracted and reflected at two interfaces. (b)-(d) show the spin-wave resonant transmission effect at $\theta_i = 0^\circ$, 10° and 20° , where the resonant peak is moved to higher frequency as θ_i increases. (e) As $\theta_i > \theta_c$, spin waves in GdIG (\mathbf{m}_2) become evanescent and then propagate into YIG (\mathbf{m}_3) in the form of plane waves, which is called the spin-wave tunnelling. The transmission spectra at $\theta_i = 30^\circ$, 60° and 89° are shown in (f)-(h). The thickness of GdIG (\mathbf{m}_2) is 10 nm.

efficients can be obtained. The transmittance T as a function of frequency $\omega/2\pi$ is shown in Figure 7(b)-(d) at different θ_i when $\theta_i < \theta_c$. The results reveal that spin waves can totally pass through GdIG (\mathbf{m}_2) at a special frequency, that is, $T = 1$, and such a phenomenon is referred to as the spin-wave resonant transmission effect. As θ_i increases, the position of the resonant peak moves to a higher frequency. The resonant transmission is general in systems with two interfaces⁴⁴⁻⁴⁷, which is closely related to the coherence of spin waves. In the present system, when the phases of ϕ_{2i} and ϕ_{2r} meet certain conditions, resonant transmission occurs.

In Figure 7(e), ϕ_{2i}^e and ϕ_{2r}^e are evanescent waves with no coherence, thus the resonant transmission does not exist. Moreover, the total reflection is also nonexistent. The evanescent waves decay along y axis in GdIG (\mathbf{m}_2) and turn into the plane waves ϕ_{3t} in YIG (\mathbf{m}_3). Such a phenomenon is referred to as spin-wave tunnelling due to the transmission being by means of the evanescent waves. Figure 7(f)-(h) show the frequency-dependent transmittance T at $\theta_i = 30^\circ$, 60° and 89° . As the frequency $\omega/2\pi$ or incident angle θ_i is increased, the decay length L_{12} de-

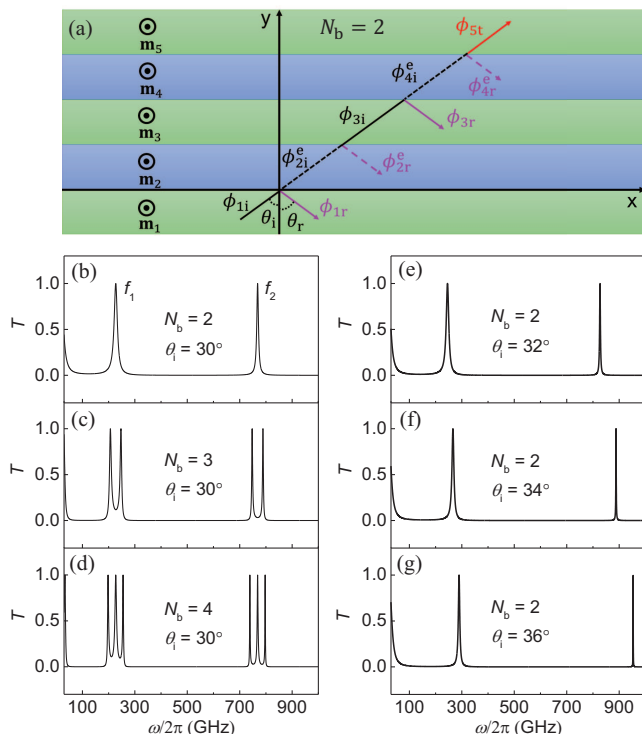


FIG. 8. The spin-wave resonant tunnelling effect when $\theta_i > \theta_c$. (a) The spin-wave propagation in YIG (\mathbf{m}_1)/GdIG (\mathbf{m}_2)/YIG (\mathbf{m}_3)/GdIG (\mathbf{m}_4)/YIG (\mathbf{m}_5) with the P configuration. The medium 2 and medium 4 are barriers and thus spin waves therein are evanescent. N_b represents the number of GdIG barriers. (b)-(d) are the transmission spectra at $\theta_i = 30^\circ$ with $N_b = 2, 3$ and 4. The number of resonant tunnelling peaks increase as N_b is increased. (e)-(g) are the transmission spectra at $N_b = 2$ with $\theta_i = 32^\circ, 34^\circ$ and 36° . The resonant tunnelling frequency increases as θ_i is increased. The thickness of GdIG (\mathbf{m}_2), YIG (\mathbf{m}_3) and GdIG (\mathbf{m}_4) are 10, 10 and 10 nm.

creases, thus the transmittance diminishes. As $\omega/2\pi$ is high enough or θ_i is close to 90° , the decay length tends to zero, leading to the total reflection.

As the number of media is further increased to five at $\theta_i > \theta_c$ as shown in Figure 8(a), another resonance effect arises, which is referred to as spin-wave resonant tunnelling effect. The difference between the resonant transmission and resonant tunnelling can be described as follows. The resonant tunnelling is a special case of the resonant transmission. If the evanescent waves are involved in the transmission process, the phenomenon of $T = 1$ is referred to as the resonant tunnelling^{42,43}. In Figure 8(b), two resonant tunnelling peaks with resonant frequency f_1 and f_2 at $N_b = 2$ and $\theta_i = 30^\circ$ can be observed, where N_b is the number of GdIG. For spin waves, GdIG (\mathbf{m}_2) and GdIG (\mathbf{m}_4) can be regarded as the potential barriers, where the plane waves are forbidden. Thus N_b also represents the number of barriers. As N_b is increased to three in Figure 8(c), the single peak at f_1 (or f_2) splits into two. In Figure 8(d), $N_b = 4$,

the single peak becomes three. The results indicate that the number of resonant tunnelling peaks depends on the number of barriers. As N_b increases, the single peak will split into $N_b - 1$. Figure 8(b) and (e)-(g) exhibit the influence of θ_i on the resonant tunnelling. Apparently, the peaks are moved to high frequency as the incident angle θ_i increases. Moreover, in Figure 8, an observation can be made that the full width at half maximum (FWHM) of the high-frequency peaks tends to be narrower. The narrow FWHM is useful in the design of the spin-wave filter, which only allows spin waves with a particular frequency to transmit.

The spin-wave transmission in multi-medium systems shows significant differences with the two-medium systems. Such differences are closely related to the number of the scattering interfaces. In two-medium systems, there is no resonance effect due to the single interface. Hence, the primary condition of resonance is the existence of at least two scattering interfaces. Meanwhile, the existence of plane waves are also essential between the two interfaces. Otherwise, like the case in Figure 7(e), the resonance cannot occur.

B. AP configuration

In this section, a discussion is provided on the spin-wave transmission in the systems with the AP configuration. The YIG (\mathbf{m}_1)/GdIG (\mathbf{m}_2) heterojunction with antiferromagnetic IEC is considered, as shown in Figure 9(a). Due to the inverse spin-wave polarization, the spin waves are all reflected back and propagate into GdIG (\mathbf{m}_2) in the form of evanescent waves ϕ_{2i}^e . Based on such a mechanism, the effects of the total reflection and decay are expected to be independent of materials, and only depend on the polarization inversion of the two magnetic media. To test such a claim, the direction of the spin-wave propagation is inverted, as shown in Figure 9(c). On the basis of Eq. (19), the reflectance $R = r_{\text{AP}}^2 \equiv 1$ can be demonstrated, including whether the direction is from YIG (\mathbf{m}_1) to GdIG (\mathbf{m}_2), or from GdIG (\mathbf{m}_2) to YIG (\mathbf{m}_1), invariably leading to the total reflection. Such inverse-polarization-induced total reflection has been presented by the previous works^{35,36}. Additionally, the results of the decay lengths $L_{12} = 1/|k_{2y}^{12}|$ and $L_{21} = 1/|k_{1y}^{21}|$ are given in Figure 9(b) and Figure 9(d), corresponding to the cases of Figure 9(a) and Figure 9(c), respectively. The incident-angle and frequency dependence of decay lengths are similar to those shown in Figure 5(b). With the increase of θ_i , both L_{12} and L_{21} decrease. As $\omega/2\pi$ is increased, the decay lengths decrease rapidly, referred to as the MSE, resembling the case of $\theta_i > \theta_c$ in the aforementioned P state. Notably, the MSE in the YIG/GdIG heterojunction with the AP configuration has been investigated in the previous research by the present author through both theoretical method and micromagnetic simulation³⁵. Further, an obvious difference of the decay length ΔL can be found at given $\omega/2\pi$

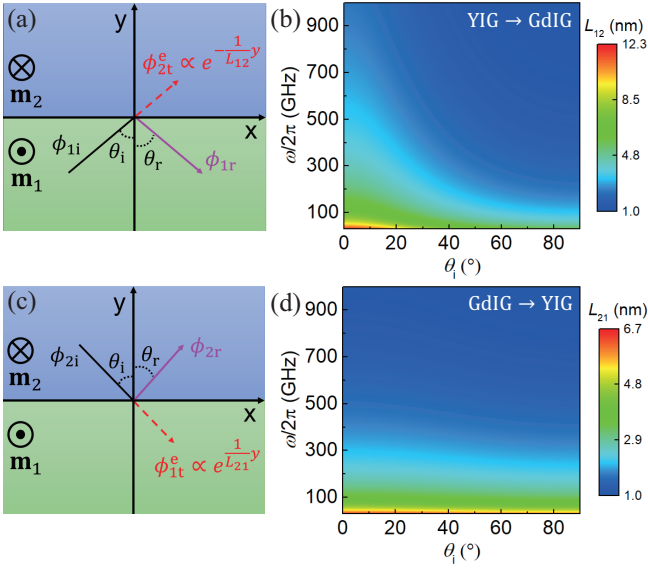


FIG. 9. The decay lengths of evanescent waves in YIG (\mathbf{m}_1)/GdIG (\mathbf{m}_2) heterojunction with the AP configuration. (a) Spin waves propagate from YIG (\mathbf{m}_1) to GdIG (\mathbf{m}_2). The waves in GdIG (\mathbf{m}_2) have the form of $e^{-\frac{y}{L_{12}}}$, which are evanescent due to the reversed spin-wave polarization compared with YIG (\mathbf{m}_1). (c) shows the case that spin waves propagate from GdIG (\mathbf{m}_2) to YIG (\mathbf{m}_1). The evanescent waves in YIG (\mathbf{m}_1) is in the form of $e^{-\frac{y}{L_{21}}}$. (b) and (d) are the calculation results of decay lengths, corresponding to the cases of (a) and (c), respectively.

and θ_i between the two paths. The formula of ΔL can be written as

$$\begin{aligned} \Delta L &= L_{21} - L_{12} = \frac{1}{|k_{1y}^{21}|} - \frac{1}{|k_{2y}^{12}|} \\ &= \frac{|k_{2y}^{12}|^2 - |k_{1y}^{21}|^2}{|k_{1y}^{21}| |k_{2y}^{12}| (|k_{2y}^{12}| + |k_{1y}^{21}|)}. \end{aligned} \quad (27)$$

The denominator is positive, and the numerator is defined as $\Delta|k|^2 = |k_{2y}^{12}|^2 - |k_{1y}^{21}|^2$. According to Eq. (14), the following can be obtained:

$$\begin{aligned} \Delta|k|^2 &= \frac{\omega}{2\gamma} \left(\frac{M_1}{A_1} - \frac{M_2}{A_2} \right) \cos^2(\theta_i) \\ &\quad + \left(\frac{K_1}{A_1} - \frac{K_2}{A_2} \right) [1 + \sin^2(\theta_i)] \end{aligned} \quad (28)$$

Thus, the conditions of $\Delta|k|^2 = 0$ ($\Delta L = 0$) are $\frac{M_1}{A_1} - \frac{M_2}{A_2} = 0$ and $\frac{K_1}{A_1} - \frac{K_2}{A_2} = 0$. In other words, $m_1^* + m_2^* = 0$ and $V_1 + V_2 = 0$. Obviously, $\Delta L \neq 0$ because $m_1^* + m_2^* \neq 0$ and $V_1 + V_2 \neq 0$ in the system, showing that the nonreciprocity of the decay lengths results from the asymmetries of the effective mass of magnons and potential energy of two media.

Figure 10(a) shows the GH shift Δ_r^{12} of the reflected spin waves. Δ_r^{12} is calculated by the equation $\Delta_r^{12} = -\frac{\partial \varphi_r}{\partial k_x}$, where $\varphi_r = \arctan[\text{Im}(r_{\text{AP}})/\text{Re}(r_{\text{AP}})]$ is the phase

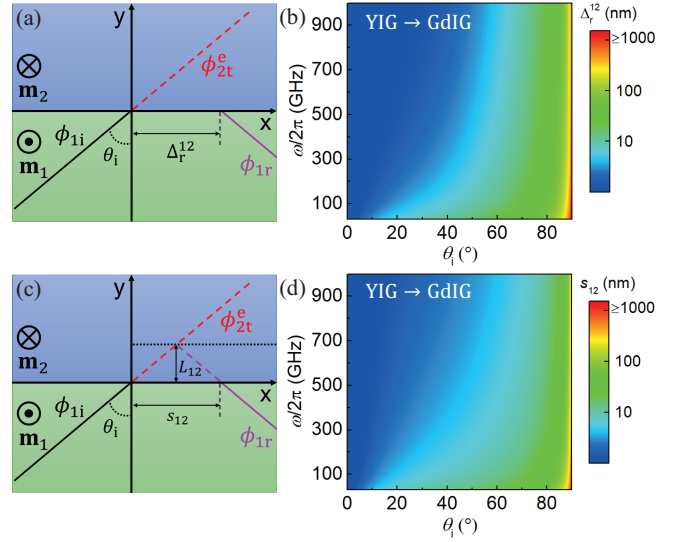


FIG. 10. The GH effect in the AP configuration as spin waves propagate from YIG (\mathbf{m}_1) to GdIG (\mathbf{m}_2). (a) shows the GH shift of the reflected waves, represented by Δ_r^{12} . (b) is the computed result of Δ_r^{12} . (c) The relationship between the lateral shift s_{12} and the decay length L_{12} . The black dot line represents the effective reflecting interface. (d) is the computed result of s_{12} . The color bars in (b) and (d) are shown in the log scale.

difference between the reflected and incident waves with $\text{Re}(r_{\text{AP}})$ and $\text{Im}(r_{\text{AP}})$ being the real and imaginary parts of the reflection coefficient r_{AP} , respectively. The computed results are shown in Figure 10(b). As θ_i increases, or $\omega/2\pi$ decreases, Δ_r^{12} becomes larger monotonically. In particular, when θ_i approaches 90° , Δ_r^{12} tends to infinity. As such, in order to obtain the precise spin-wave path, the GH shift must be taken into consideration.

The shift s_{12} is subsequently calculated by the equation $s_{12} = 2L_{12} \tan(\theta_i)$ to investigate the connection with the GH shift Δ_r^{12} . Figure 10(c) shows the relationship between s_{12} and the decay length L_{12} . The spin waves are not reflected at x axis, but propagate into GdIG in the form of decay and are reflected at another effective interface marked by the black dot line. Such a mechanism contributes to the positive lateral shift s_{12} . The computed results of s_{12} are given in Figure 10(d). By comparing Figure 10(b) and Figure 10(d), an observation can be made that the incident-angle and frequency dependence of Δ_r^{12} and s_{12} are the same, despite a slight difference in magnitude. At the same time, the distinction of Δ_r^{12} and s_{12} in magnitudes indicates that the exact reflecting interface is not the black dot line, but in the vicinity of said line. Thus, the decay length is approximately equal to the real penetration depth of spin waves in GdIG. Similar to the P state, the similarity between Δ_r^{12} and s_{12} is applicable only in the case that the IEC between YIG and GdIG is strong. Besides, when spin waves propagate from GdIG to YIG, the results of Δ_r^{12} and s_{21} are analogous to Figure 10, which are shown in

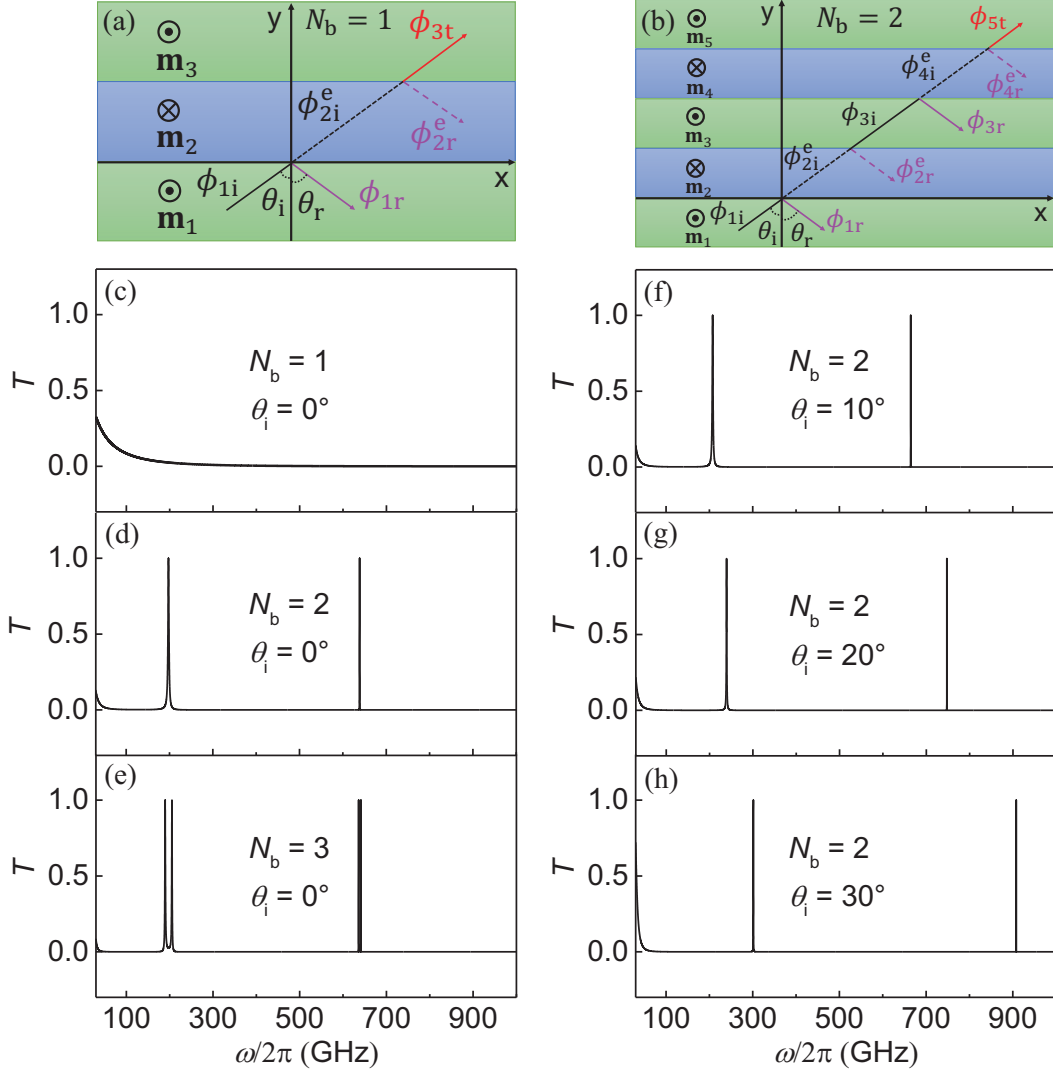


FIG. 11. The spin-wave tunnelling and resonant tunnelling effect in the multi-medium system with the AP configuration. (a) The spin-wave tunnelling in YIG (\mathbf{m}_1)/GdIG (\mathbf{m}_2)/YIG (\mathbf{m}_3), which is the single barrier structure ($N_b = 1$). The thickness of GdIG (\mathbf{m}_2) is 10 nm. (b) is the $N_b = 2$ case, corresponding to the structure YIG (\mathbf{m}_1)/GdIG (\mathbf{m}_2)/YIG (\mathbf{m}_3)/GdIG (\mathbf{m}_4)/YIG (\mathbf{m}_5), where the spin-wave resonant tunnelling occurs. (c)-(e) are the transmission spectra at $\theta_i = 0^\circ$ with $N_b = 1, 2$ and 3. (f)-(h) are the transmission spectra at $N_b = 2$ with $\theta_i = 10^\circ, 20^\circ$ and 30° . The thickness of GdIG (\mathbf{m}_2), YIG (\mathbf{m}_3) and GdIG (\mathbf{m}_4) are 10, 10 and 10 nm.

the Supplemental Material⁷⁰.

The spin-wave transmission in multi-medium systems with the AP configuration is also investigated. Figure 11(a) and (b) show the YIG (\mathbf{m}_1)/GdIG (\mathbf{m}_2)/YIG (\mathbf{m}_3) and YIG (\mathbf{m}_1)/GdIG (\mathbf{m}_2)/YIG (\mathbf{m}_3)/GdIG (\mathbf{m}_4)/YIG (\mathbf{m}_5) heterostructures, corresponding to the number of GdIG barriers $N_b = 1$ and $N_b = 2$, respectively. Spin waves propagate in the form of evanescent waves in GdIG, but they are plane waves in YIG, due to the inverse spin-wave polarization. Figure 11(c) is the computed result in the case of $N_b = 1$ and $\theta_i = 0^\circ$. The nonzero transmittance T demonstrates that spin waves indeed pass through the GdIG barrier. As the frequency is increased, the decay length becomes shorter in GdIG,

and thus the transmittance decreases monotonically. For $N_b = 2$, the transmission spectra are shown in Figure 11(d), where the resonant tunnelling effect appears. Spin waves can fully transmit across the two GdIG barriers at the resonant frequency. For $N_b = 3$, as shown in Figure 11(e), the resonant peaks split. The number of splitting is $N_b - 1$ for every single peak as $N_b > 2$. Figure 11(f)-(h) shows the influence of θ_i on the resonant tunnelling. As θ_i is increased, the resonant peaks are moved to high-frequency ranges. In addition, the FWHM of the resonant peaks in Figure 11 are much narrower than those of the P configuration in Figure 8.

By comparing the spin-wave characteristics in P and AP configurations, the differences and similarities can be

observed. In the P configuration, the critical angle θ_c is vital. For $\theta_i < \theta_c$, there is no decay process of spin waves in all of the media. The refraction and reflection are the key phenomena here. Moreover, if the number of scattering interfaces is increased to two or more, resonant transmission occurs. Contrastingly, in the case of $\theta_i > \theta_c$, evanescent waves appear, leading to entirely different features, such as total reflection, decay, positive GH shift, tunnelling and resonant tunnelling effect. In the AP configuration, spin waves show considerably similar characteristics with the $\theta_i > \theta_c$ case of the P configuration. Although the aforementioned phenomena are various and complex, several traces can be found, as well as connections therebetween.

IV. CONCLUSION

In summary, a theoretical method was developed for the transmission of spin waves with nanoscale wavelengths in the P and AP magnetic configurations. Through the method, the transmission and reflection coefficients were both analytically and numerically investigated. The computed results show several phenomena, including spin-wave refraction, total reflection, decay, positive GH shifts, tunneling, resonant transmission and resonant tunneling. When the incident angle is smaller than the critical angle, the spin-wave polarization is a significant factor in the different performances of the two configurations, demonstrating that the same polarization leads to transmission while the inverse polar-

ization results in total reflection. Such effect is similar to the spin-dependent scattering in GMR^{1,2}, TMR³⁻⁵ and MVE^{20,21}. Hence, in the present study, the spin-wave scattering process in P ($\theta_i < \theta_c$) and AP configurations can be referred to as polarization-dependent scattering. As the incident angle exceeds the critical angle, the situation in the P configuration is significantly changed and shows similarities with the AP case. The transmitted spin waves turn into evanescent waves, of which the decay lengths were explored and a connection with the positive GH shifts was found. Moreover, the investigation of spin waves propagating in multi-medium systems displays the resonance effect, which is closely related to the spin-wave coherence. The present study can facilitate further understanding of the transmission of spin waves in different magnetic configurations and can provide guidance for the design of future magnonic devices.

ACKNOWLEDGMENTS

We thank T. Y. Zhang for helpful discussions. This work was supported by the National Key Research and Development Program of China [MOST, Grants No. 2017YFA0206200 and 2021YFB3201801], the National Natural Science Foundation of China [NSFC, Grants No.51831012 and No.51620105004], Beijing Natural Science Foundation (Grant No. Z201100004220006) and partially supported by the Strategic Priority Research Program (B) [Grant No. XDB33000000] of the Chinese Academy of Sciences (CAS).

* These two authors contributed equally to this work.

† xfhan@iphy.ac.cn

¹ M. N. Baibich, J. M. Broto, A. Fert, F. N. Van Dau, F. Petroff, P. Etienne, G. Creuzet, A. Friederich, and J. Chazelas, *Physical Review Letters* **61**, 2472 (1988).

² G. Binash, P. Grünberg, F. Saurenbach, and W. Zinn, *Physical Review B* **39**, 4828 (1989).

³ M. Julliere, *Physics Letters A* **54**, 225 (1975).

⁴ T. Miyazaki and N. Tezuka, *Journal of Magnetism and Magnetic Materials* **139**, L231 (1995).

⁵ J. S. Moodera, L. R. Kinder, T. M. Wong, and R. Meservey, *Physical Review Letters* **74**, 3273 (1995).

⁶ S. M. Thompson, *Journal of Physics D: Applied Physics* **41**, 093001 (2008).

⁷ B. Dieny, V. S. Speriosu, S. S. P. Parkin, B. A. Gurney, D. R. Wilhoit, and D. Mauri, *Physical Review B* **43**, 1297 (1991).

⁸ B. Dieny, V. S. Speriosu, S. Metin, S. S. P. Parkin, B. A. Gurney, P. Baumgart, and D. R. Wilhoit, *Journal of Applied Physics* **69**, 4774 (1991).

⁹ B. Dieny, V. S. Speriosu, B. A. Gurney, S. S. P. Parkin, D. R. Wilhoit, K. P. Roche, S. Metin, D. T. Peterson, and S. Nadimi, *Journal of Magnetism and Magnetic Materials* **93**, 101 (1991).

¹⁰ B. Dieny, *Journal of Magnetism and Magnetic Materials* **136**, 335 (1994).

¹¹ V. V. Kruglyak and R. J. Hicken, *Journal of Magnetism and Magnetic Materials* **306**, 191 (2006).

¹² S. Neusser, B. Botters, and D. Grundler, *Physical Review B* **78**, 054406 (2008).

¹³ A. A. Serga, A. V. Chumak, and B. Hillebrands, *Journal of Physics D: Applied Physics* **43**, 264002 (2010).

¹⁴ V. V. Kruglyak, S. O. Demokritov, and D. Grundler, *Journal of Physics D: Applied Physics* **43**, 264001 (2010).

¹⁵ A. V. Chumak, V. I. Vasyuchka, A. A. Serga, and B. Hillebrands, *Nature Physics* **11**, 453 (2015).

¹⁶ M. P. Kostylev, A. A. Serga, T. Schneider, B. Leven, and B. Hillebrands, *Physical Review Letters* **87**, 153501 (2005).

¹⁷ T. Schneider, A. A. Serga, B. Leven, B. Hillebrands, R. L. Stamps, and M. P. Kostylev, *Applied Physics Letters* **92**, 022505 (2008).

¹⁸ S.-K. Kim, K.-S. Lee, and D.-S. Han, *Applied Physics Letters* **95**, 082507 (2009).

¹⁹ A. V. Chumak, A. A. Serga, and B. Hillebrands, *Nature Communications* **5**, 4700 (2014).

²⁰ H. Wu, L. Huang, C. Fang, B. S. Yang, C. H. Wan, G. Q. Yu, J. F. Feng, H. X. Wei, and X. F. Han, *Physical Review Letters* **120**, 097205 (2018).

²¹ C. Luo, C. H. Wan, X. Wang, C. Fang, P. Tang, W. J. Kong, M. K. Zhao, L. N. Jiang, B. S. Tao, G. Q. Yu, and

- X. F. Han, *Physical Review B* **98**, 134426 (2018).
- ²² Q. Wang, P. Pirro, R. Verba, A. Slavin, B. Hillebrands, and A. V. Chumak, *Science Advances* **4**, e1701517 (2018).
- ²³ C. Liu, S. Wu, J. Zhang, J. Chen, J. Ding, J. Ma, Y. Zhang, Y. Sun, S. Tu, H. Wang, P. Liu, C. Li, Y. Jiang, P. Gao, D. Yu, J. Xiao, R. Duine, M. Wu, C.-W. Nan, J. Zhang, and H. Yu, *Nature Nanotechnology* **14**, 691 (2019).
- ²⁴ J. Chen, T. Yu, C. Liu, T. Liu, M. Madami, K. Shen, J. Zhang, S. Tu, M. S. Alam, K. Xia, M. Wu, G. Gubbiotti, Y. M. Blanter, G. E. W. Bauer, and H. Yu, *Physical Review B* **100**, 104427 (2019).
- ²⁵ Q. Wang, T. Brächer, M. Mohseni, B. Hillebrands, V. I. Vasyuchka, A. V. Chumak, and P. Pirro, *Applied Physics Letters* **115**, 092401 (2019).
- ²⁶ Z. Zhang, M. Vogel, J. Holanda, M. B. Jungfleisch, C. Liu, Y. Li, J. E. Pearson, R. Divan, W. Zhang, A. Hoffmann, Y. Nie, and V. Novosad, *Applied Physics Letters* **115**, 232402 (2019).
- ²⁷ C. Y. Guo, C. H. Wan, W. Q. He, M. K. Zhao, Z. R. Yan, Y. W. Xing, X. Wang, P. Tang, Y. Z. Liu, S. Zhang, Y. W. Liu, and X. F. Han, *Nature Electronics* **3**, 304 (2020).
- ²⁸ Y. I. Gorobets and S. A. Reshetnyak, *Technical Physics* **43**, 188 (1998).
- ²⁹ H. Xi, X. Wang, Y. Zheng, and P. J. Ryan, *Journal of Applied Physics* **104**, 063921 (2008).
- ³⁰ K. Tanabe, R. Matsumoto, J.-i. Ohe, S. Murakami, T. Moriyama, D. Chiba, K. Kobayashi, and T. Ono, *Applied Physics Express* **7**, 053001 (2014).
- ³¹ W. Yu, J. Lan, R. Wu, and J. Xiao, *Physical Review B* **94**, 140410 (2016).
- ³² J. Stigloher, M. Decker, H. S. Körner, K. Tanabe, T. Moriyama, T. Taniguchi, H. Hata, M. Madami, G. Gubbiotti, K. Kobayashi, T. Ono, and C. H. Back, *Physical Review Letters* **117**, 037204 (2016).
- ³³ J. Mulkers, B. Van Waeyenberge, and M. V. Milošević, *Physical Review B* **97**, 104422 (2018).
- ³⁴ S. Mieszczak, O. Busel, P. Gruszecki, A. N. Kuchko, J. W. Klos, and M. Krawczyk, *Physical Review Applied* **13**, 054038 (2020).
- ³⁵ Z. R. Yan, Y. W. Xing, and X. F. Han, *Physical Review B* **104**, L020413 (2021).
- ³⁶ V. D. Poimanov and V. V. Kruglyak, *Journal of Applied Physics* **130**, 133902 (2021).
- ³⁷ Y. S. Dadoenkova, N. N. Dadoenkova, I. L. Lyubchanskii, M. L. Sokolovskyy, J. W. Klos, J. Romero-Vivas, and M. Krawczyk, *Applied Physics Letters* **101**, 042404 (2012).
- ³⁸ P. Gruszecki, Y. S. Dadoenkova, N. N. Dadoenkova, I. L. Lyubchanskii, J. Romero-Vivas, K. Y. Guslienko, and M. Krawczyk, *Physical Review B* **92**, 054427 (2015).
- ³⁹ P. Gruszecki, M. Mailyan, O. Gorobets, and M. Krawczyk, *Physical Review B* **95**, 014421 (2017).
- ⁴⁰ Z. Wang, Y. Cao, and P. Yan, *Physical Review B* **100**, 064421 (2019).
- ⁴¹ S. O. Demokritov, A. A. Serga, A. Andriy, V. E. Demidov, M. P. Kostylev, B. Hillebrands, and A. N. Slavin, *Physical Review Letters* **93**, 047201 (2004).
- ⁴² U.-H. Hansen, M. Gatzert, V. E. Demidov, and S. O. Demokritov, *Physical Review Letters* **99**, 127204 (2007).
- ⁴³ P. Tang and X. F. Han, *Physical Review B* **99**, 054401 (2019).
- ⁴⁴ M. P. Kostylev, A. A. Serga, T. Schneider, T. Neumann, B. Leven, B. Hillebrands, and R. L. Stamps, *Physical Review B* **76**, 184419 (2007).
- ⁴⁵ H. Xi and S. Xue, *Journal of Applied Physics* **101**, 123905 (2007).
- ⁴⁶ Y. W. Xing, Z. R. Yan, and X. F. Han, *Physical Review B* **103**, 054425 (2021).
- ⁴⁷ H. Qin, R. B. Holländer, L. Flajšman, F. Hermann, R. Dreyer, G. Woltersdorf, and S. van Dijken, *Nature Communications* **12**, 2293 (2021).
- ⁴⁸ B. Lenk, H. Ulrichs, F. Garbs, and M. Münzenberg, *Physics Reports* **507**, 107 (2011).
- ⁴⁹ K. Di, S. X. Feng, S. N. Piramanayagam, V. L. Zhang, H. S. Lim, S. C. Ng, and M. H. Kuok, *Scientific Reports* **5**, 10153 (2015).
- ⁵⁰ J. M. Gomez-Perez, S. Vélez, L. McKenzie-Sell, M. Amado, J. Herrero-Martín, J. López-López, S. Blanco-Canosa, L. E. Hueso, A. Chuvilin, J. W. A. Robinson, and F. Casanova, *Physical Review Applied* **10**, 044046 (2018).
- ⁵¹ L. Landau and E. Lifshitz, “3 - on the theory of the dispersion of magnetic permeability in ferromagnetic bodies reprinted from *physikalische zeitschrift der sowjetunion* 8, part 2, 153, 1935,” in *Perspectives in Theoretical Physics*, edited by L. P. Pitaevski (Pergamon, Amsterdam, 1992) pp. 51–65.
- ⁵² T. L. Gilbert, *IEEE Transactions on Magnetics* **40**, 3443 (2004).
- ⁵³ A. G. Gurevich and G. A. Melkov, *Magnetization oscillations and waves* (CRC press, 2020).
- ⁵⁴ Y. I. Gorobets and S. A. Reshetnyak, *Technical Physics* **43**, 188 (1998).
- ⁵⁵ P. Yan, X. S. Wang, and X. R. Wang, *Physical Review Letters* **107**, 177207 (2011).
- ⁵⁶ W. Wang, M. Albert, M. Beg, M.-A. Bisotti, D. Chernyshenko, D. Cortés-Ortuño, I. Hawke, and H. Fangohr, *Physical Review Letters* **114**, 087203 (2015).
- ⁵⁷ J. Lan, W. Yu, R. Wu, and J. Xiao, *Physical Review X* **5**, 041049 (2015).
- ⁵⁸ S.-J. Lee, J.-H. Moon, H.-W. Lee, and K.-J. Lee, *Physical Review B* **96**, 184433 (2017).
- ⁵⁹ C. Jia, D. Ma, A. F. Schäffer, and J. Berakdar, *Nature Communications* **10**, 2077 (2019).
- ⁶⁰ S. A. Reshetnyak, *Physics of the Solid State* **46**, 1061 (2004).
- ⁶¹ S.-K. Kim, S. Choi, K.-S. Lee, D.-S. Han, D.-E. Jung, and Y.-S. Choi, *Applied Physics Letters* **92**, 212501 (2008).
- ⁶² Z. R. Yan, C. H. Wan, and X. F. Han, *Physical Review Applied* **14**, 044053 (2020).
- ⁶³ J. Xiao and G. E. W. Bauer, *Physical Review Letters* **108**, 217204 (2012).
- ⁶⁴ S. Klingler, A. V. Chumak, T. Mewes, B. Khodadadi, C. Mewes, C. Dubs, O. Surzhenko, B. Hillebrands, and A. Conca, *Journal of Physics D: Applied Physics* **48**, 015001 (2014).
- ⁶⁵ A. V. Chumak, A. A. Serga, and B. Hillebrands, *Journal of Physics D: Applied Physics* **50**, 244001 (2017).
- ⁶⁶ M. Shimada, *Japanese Journal of Applied Physics* **11**, 964 (1972).
- ⁶⁷ H. Lassri, E. K. Hlil, S. Prasad, and R. Krishnan, *Journal of Solid State Chemistry* **184**, 3216 (2011).
- ⁶⁸ M. Althammer, *Journal of Physics D: Applied Physics* **51**, 313001 (2018).
- ⁶⁹ M. Vohl, J. Barnaś, and P. Grünberg, *Physical Review B* **39**, 12003 (1989).
- ⁷⁰ See Supplemental Material at the link for more details.
- ⁷¹ V. Ruddy, *Fiber and Integrated Optics* **9**, 143 (1990).
- ⁷² V. Ruddy, B. D. MacCraith, and J. A. Murphy, *Journal of Applied Physics* **67**, 6070 (1990).
- ⁷³ S. Harlepp, J. Robert, N. C. Darnton, and D. Chatenay, *Applied Physics Letters* **85**, 3917 (2004).
- ⁷⁴ M. Milosevic, *Applied Spectroscopy* **67**, 126 (2013).

- ⁷⁵ H. Yamamoto, Y. Kanie, H. Sano, and K. Taniguchi,
physica status solidi (b) **169**, K17 (1992).
- ⁷⁶ C. L. Roy and A. Khan,
physica status solidi (b) **176**, 101 (1993).